International Journal of Fatigue 61 (2014) 151–159

Contents lists available at ScienceDirect

International Journal of Fatigue

journal homepage: www.elsevier.com/locate/ijfatigue

Prediction of non-proportionality factors of multiaxial histories using the Moment Of Inertia method

Marco Antonio Meggiolaro *, Jaime Tupiassú Pinho de Castro

Department of Mechanical Engineering, Pontifical Catholic University of Rio de Janeiro, Rua Marquês de São Vicente 225 – Gávea, Rio de Janeiro, RJ 22451-900, Brazil

ARTICLE INFO

Article history:
Received 31 October 2012
Received in revised form 8 November 2013
Accepted 19 November 2013
Available online 1 December 2013

Keywords:
Multiaxial fatigue
Non-proportional loadings
Non-proportionality factor
Additional hardening
Equivalent ranges

ABSTRACT

This work studies further an approach originally proposed to evaluate equivalent stress and strain ranges in non-proportional (NP) load histories, called the Moment Of Inertia (MOI) method. The MOI method assumes that the path contour in the deviatoric stress or strain diagram is a homogeneous wire with unit mass. The center of mass of such wire gives then the mean component of the path, while the moments of inertia of the wire can be used to obtain the equivalent stress or strain ranges. The MOI method is an alternative to convex enclosure methods, such as Dang Van's Minimum Ball or the Maximum Prismatic Hull methods, without the need for computationally-intensive search algorithms or adjustable parameters. The MOI method is extended here to calculate as well the non-proportionality factor F_{np} of generic multiaxial load histories, formulated in an alternative sub-space of the deviatoric plastic strains. Experimental results for 14 different multiaxial histories prove the effectiveness of the MOI method to predict the observed non-proportionality factors. Hence, it can be a most useful tool for the computation of multiaxial fatigue damage in practical applications.

1. Introduction

Several multiaxial fatigue damage models have been introduced in the literature, such as the ones proposed by Sines, Crossland, Findley, McDiarmid, Brown–Miller, Fatemi–Socie and Smith–Watson–Topper (SWT) [1]. All of them require some measure of an equivalent stress or strain range, which may be difficult to obtain for non-proportional (NP) multiaxial load histories.

For a given multiaxial stress–strain NP history, the fatigue damage can be calculated by projecting the history onto a candidate plane at the critical point [1]. This critical plane approach is simple to compute for Case A cracks, which initiate perpendicular to the free surface. In this case, the in-plane shear stress or strain may be counted using a uniaxial rainflow algorithm [2]. On the other hand, for Case B cracks, which initiate at a 45° angle from the free surface, a multiaxial rainflow count must be performed to identify individual cycles formed by the in-plane and out-of-plane shear components [3].

For each rainflow-counted cycle, the equivalent stress or strain range is often computed using the so-called convex enclosure methods [4], which try to find circles, ellipses or rectangles that contain the entire projected path in the 2D case, or hyperspheres, hyperellipsoids or hyperprisms in a generic 5-dimensional (5D) equivalent stress space. The traditional convex enclosure methods have been reviewed in [4]: the Minimum Ball, Minimum Circumscribed Ellipsoid, Minimum Volume Ellipsoid, Minimum F-norm Ellipsoid (MFE), Maximum Prismatic Hull and Maximum Volume Prismatic Hull. These methods make use of stress and strain parameters such as the von Mises stress and strain ranges $\Delta\sigma_{Mises}$ and $\Delta\varepsilon_{Mises}$, defined by:

$$\Delta\sigma_{Mises}=\frac{\sqrt{(\Delta\sigma_x-\Delta\sigma_y)^2+(\Delta\sigma_x-\Delta\sigma_z)^2+(\Delta\sigma_y-\Delta\sigma_z)^2+6(\Delta\tau_{xy}^2+\Delta\tau_{xz}^2+\Delta\tau_{yz}^2)}}{\sqrt{2}} \tag{1}$$

$$\Delta\varepsilon_{Mises}=\frac{\sqrt{(\Delta\varepsilon_x-\Delta\varepsilon_y)^2+(\Delta\varepsilon_x-\Delta\varepsilon_z)^2+(\Delta\varepsilon_y-\Delta\varepsilon_z)^2+1.5(\Delta\gamma_{xy}^2+\Delta\gamma_{xz}^2+\Delta\gamma_{yz}^2)}}{\sqrt{2}\cdot(1+\bar{\nu})} \tag{2}$$

where the $\bar{\nu}$ is the mean (or effective) Poisson coefficient $\bar{\nu}=(0.5\varepsilon_p+\nu_e\varepsilon_e)/(\varepsilon_p+\varepsilon_e)$, while ε_e and ε_p are the elastic and plastic components of the strains, and ν_e and ν_p are the elastic and plastic Poisson coefficients ($\nu_p=0.5$ assuming plastic strains conserve material volume).

Extensive simulations from [4] showed that all convex enclosure methods can lead to poor predictions of the *mean* stresses or strains, if they are assumed as located at the center of the ball, ellipse or prism, as seen in Fig. 1(a), which shows a stress path shaped very differently from an ellipse and its Minimum F-norm Ellipsoid (MFE) enclosure. Convex enclosure methods may also

* Corresponding author. Tel.: +55 21 3527 1424; fax: +55 21 3527 1165.
E-mail addresses: meggi@puc-rio.br (M.A. Meggiolaro), jtcastro@puc-rio.br (J.T.P. Castro).

0142-1123/$ - see front matter © 2013 Elsevier Ltd. All rights reserved.
http://dx.doi.org/10.1016/j.ijfatigue.2013.11.016

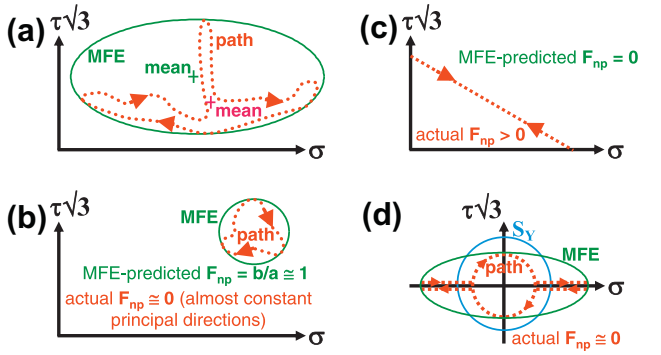

Fig. 1. History path examples showing the inadequacy of convex enclosure methods, such as the Minimum F-norm Ellipsoid (MFE), to predict mean components or the non-proportionality factor F_{np}.

result in poor estimates of stress or strain *amplitudes*, in special for highly non-convex NP history paths, such as cross or star-shaped paths.

If only the stress or strain history is measured, then an incremental plasticity algorithm must be implemented to obtain the stress–strain behavior caused by a NP loading. To account for NP hardening effects, it is necessary to correctly evaluate the non-proportionality factor F_{np} associated with the load history and the additional hardening coefficient α_{np}. The factor F_{np} depends solely on the shape of the history path [5], while α_{np} depends not only on the material and its microstructure, but also on the strain amplitudes involved in the history. The additional hardening coefficient can be estimated from

$$\alpha_{np} = \frac{\sigma_{OP}}{\sigma_{IP}} - 1 \tag{3}$$

where σ_{IP} and σ_{OP} are the equivalent von Mises stress amplitudes obtained under the same strain level for, respectively, in-phase ($F_{np} = 0$) and 90° out-of-phase ($F_{np} = 1$) loadings. This σ_{OP}/σ_{IP} ratio is usually calculated at high plastic strains, however it can be defined at any strain level, resulting in some strain amplitude dependence of α_{np}.

If α_{np} is eliminated from the F_{np} equation, then F_{np} can be obtained for a given von Mises stress amplitude σ from

$$F_{np} = \frac{(\sigma/\sigma_{IP}) - 1}{(\sigma_{OP}/\sigma_{IP}) - 1} \tag{4}$$

as long as σ is measured in the same material and under a similar strain level as the one from the σ_{IP} and σ_{OP} measurements. Using the above equation, F_{np} can be calculated from experiments without the need to explicitly obtain α_{np} or to worry about its strain amplitude dependence. In the absence of experimental data to measure σ, σ_{IP} and σ_{OP}, the NP factor F_{np} must be estimated from the load history path. The main F_{np} estimates are presented next.

2. Estimates of the non-proportionality factor F_{np}

Originally, F_{np} was estimated from the aspect ratio of the convex enclosure that contains the history path (e.g. the aspect ratio b/a of an enclosing ellipse with semi-axes a and b). But such convex enclosure estimates can lead to poor predictions of F_{np}, as seen in Fig. 1(b). This example shows a path that does not encircle the origin of the von Mises $\sigma \times \tau\sqrt{3}$ diagram, while entirely located far away from it. Despite the almost circular shape of the enclosing Minimum F-norm Ellipsoid (MFE), which would suggest $F_{np} \cong 1$, the principal direction in fact varies very little along such path, since the angle between each point in the path and the origin of the 2D diagram varies very little during each cycle – thus, the actual F_{np} should be very small in this example.

Another notable example where convex enclosures fail to calculate F_{np} is shown in Fig. 1(c), where a loading path describes a straight line that does not cross the origin of the diagram. This particular path induces a 45° variation of the principal direction, implying in F_{np} *0*, however any convex enclosure method would predict $F_{np} = 0$ for such straight line. This path is an interesting example of how an in-phase loading (which is represented by a straight path) can be non-proportional (making the principal direction vary). Note also that convex enclosure methods can lead to poor F_{np} predictions even in paths that encircle the origin, in special when the path shape is very different from an ellipse or rectangle, or when the mean value of the path is not located close to the origin.

The use of the stress path to estimate F_{np} is also questionable. Fig. 1(d) shows a stress path that combines a purely elastic tension–torsion portion (well inside the yield surface with radius S_Y) with uniaxial tension–compression plastic straining. Since NP hardening is caused by plastic straining, the purely elastic portion should not influence the value of F_{np}. As plastic strains only occur along such path under uniaxial conditions, it is expected that $F_{np} = 0$, which is confirmed by experiments and incremental plasticity simulations using Tanaka's NP model [6]. However, a convex enclosure method applied to such stress path would wrongfully predict F_{np} much greater than zero, as suggested by the MFE ellipse in Fig. 1(d). Therefore, any accurate F_{np} estimation method should be based on the plastic strain path, not on the stress or total strain path.

Several methods have been proposed to estimate F_{np}, besides the ones based on convex enclosures. Kanazawa et al. [7] estimated F_{np} as a rotation factor, defined by the ratio between the shear strain range at 45° from the maximum shear plane and the maximum shear strain range. This factor correctly tends to the limits $F_{np} = 0$ for proportional loadings and $F_{np} = 1$ for 90° out-of-phase strain histories (assuming the relation $\gamma_a = (1 + \bar{\nu}) \cdot \varepsilon_a$ between strain amplitudes for Case A cracks [1]). But it fails to correctly compute F_{np} for more complex histories.

Itoh et al. [8] estimated F_{np} using an integral definition along the strain path:

$$F_{np} = \frac{\pi}{2T\varepsilon_{Imax}} \int_0^T \varepsilon_I(t) \cdot |\sin \xi(t)| \cdot dt \tag{5}$$

where $\varepsilon_I(t)$ is the absolute value of the maximum principal strain at each instant t, ε_{Imax} is the maximum value of $\varepsilon_I(t)$ along the entire path, $\xi(t)$ is the angle between the principal directions associated with $\varepsilon_I(t)$ and ε_{Imax}, and T is the time period of the path.

Itoh's method works for simple 2D (e.g. tension–torsion) histories, but it should not be applied to more general 3D to 6D histories, since it is based on a scalar measure, the angle $\xi(t)$. For instance, if the directions of $\varepsilon_I(t)$ along a load path describe a cone with symmetry axis in the direction of ε_{Imax}, then $\xi(t)$ would be constant and equal to half the cone apex angle, regardless of the chosen path. Constant amplitude or 90° out-of-phase cycles could result in the same $\xi(t)$ and $\varepsilon_I(t)$ histories, wrongfully calculating the same F_{np} for both cases. Instead of using the scalar measure $\xi(t)$, the direction of $\varepsilon_I(t)$ would need to be defined by a vector of at least two elements to be able to distinguish between these example paths.

To calculate F_{np} of a more general 6D load path, Bishop [9] introduced a 6×6 inertia tensor termed the Rectangular Moment Of Inertia (RMOI) of the stress path, which can be expressed using Voigt-Mandel's stress representation $\bar{\sigma} \equiv \left[\sigma_x \quad \sigma_y \quad \sigma_z \quad \tau_{xy}\sqrt{2} \quad \tau_{xz}\sqrt{2} \quad \tau_{yz}\sqrt{2}\right]^T$ by

$$I_\sigma \equiv \frac{1}{p_\sigma} \cdot \oint (\bar{\sigma} - \bar{\sigma}_m) \cdot (\bar{\sigma} - \bar{\sigma}_m)^T \cdot |d\bar{\sigma}| \tag{6}$$

where the mean component $\bar{\sigma}_m$ and accumulated stress p_σ are also integrated along the stress path, calculated from

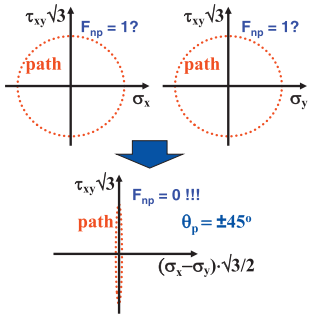

Fig. 2. An apparently 90° out-of-phase tension–torsion history can be proportional if subjected to a biaxial state $\sigma_y = \sigma_x$.

$$\bar{\sigma}_m \equiv \frac{1}{p_\sigma} \cdot \oint \bar{\sigma} \cdot |d\bar{\sigma}| \text{ and } p_\sigma \equiv \oint |d\bar{\sigma}| \tag{7}$$

In the above equations, $|d\bar{\sigma}|$ stands for the Euclidean norm of the stress increment $d\bar{\sigma}$, and the superscript T means transpose of a vector.

The RMOI stress tensor measures the distribution of the stress path, relative to its mean, about the coordinate planes. Bishop proposed that F_{np} can be estimated from the two largest eigenvectors $\lambda_{\sigma 1}$ and $\lambda_{\sigma 2}$ of I_σ ($\lambda_{\sigma 1} \geqslant \lambda_{\sigma 2}$) through

$$F_{np} = \sqrt{\lambda_{\sigma 2}/\lambda_{\sigma 1}} \tag{8}$$

Note that the normalization term $1/p_\sigma$ was not included in Bishop's original definition of I_σ, however it has been introduced here to simplify the comparison between the MOI and Bishop's methods.

Despite being more general than Itoh's method, Bishop's RMOI approach has several issues: (i) it is formulated in a stress space, instead of a more appropriate plastic strain space to deal with the path from Fig. 1(d), as discussed before; (ii) it uses a 6D formulation instead of a 5D deviatoric one, therefore it implicitly assumes that the hydrostatic component may influence F_{np}, which is non-sense for materials with pressure-insensitive yield functions such as von Mises'; (iii) it calculates the moments of inertia relative to the mean component of the load path, which would wrongfully predict $F_{np} = 0$ for the path from Fig. 1(c), instead of an $F_{np} > 0$ that would be obtained from moments relative to the origin of the coordinate axes; and (iv) it wrongfully predicts $F_{np} = 1$ for tension–torsion stress paths that describe a circle in a $\sigma \times \tau\sqrt{2}$ diagram, and not for the well-known 90° out-of-phase paths that describe a circle in the $\sigma \times \tau\sqrt{3}$ von Mises diagram.

In summary, an accurate F_{np} estimate should be: (i) formulated in the plastic strain space; (ii) independent of mean components of stresses and strains; and (iii) independent of hydrostatic components. The issue with hydrostatic components can be seen in the load path from Fig. 2, which shows a 90° out-of-phase traction-torsion stress history $\sigma \times \tau\sqrt{3}$ in a biaxial state $\sigma_y = \sigma_x$. This history describes circles in both $\sigma_x \times \tau_{xy}\sqrt{3}$ and $\sigma_y \times \tau_{xy}\sqrt{3}$ diagrams, suggesting a highly non-proportional history. However, such a history would be proportional since the principal stress directions $\theta_p = \pm 45°$ are constant, because $\sigma_y = \sigma_x$ implies that $\tan\theta p = \eta_{xy}/(\sigma_x - \sigma_y) \to \pm\infty$, see Fig. 2. Thus, the non-proportionality of the loading can only be ascertained when the history is represented in a diagram based on a sub-space of the deviatoric stresses and strains, e.g. $(\sigma_x - \sigma_y) \times \tau_{xy}\sqrt{3}$ for stresses or $(\varepsilon_x - \varepsilon_y)$ - $\times \gamma_{xy}/\sqrt{3}$ for strains. These diagrams are not influenced by the hydrostatic components of the load path, since $(\sigma_x - \sigma_y) \equiv (S_x - S_y)$ and $(\varepsilon_x - \varepsilon_y) \equiv (e_x - e_y)$, where S and e stand for deviatoric stresses and strains.

Nevertheless, most F_{np} estimates are based on diagrams involving a single normal component σ_x or ε_x and a shear component τ_{xy} or γ_{xy}. Usually, the contribution of σ_y or ε_y, the normal history perpendicular to the considered x direction, is overlooked in the calculation of F_{np}. This can lead to very large errors.

To compensate for the flaws in Itoh's, Bishop's and other estimates in such cases, the Moment Of Inertia (MOI) method, originally proposed in [4] to predict equivalent stress and strain ranges, is here extended to estimate F_{np} in general 6D NP histories. The MOI method is discussed next.

3. The Moment Of Inertia (MOI) method

3.1. Calculation of alternate and mean components

The Moment Of Inertia (MOI) method has been proposed in [4] to calculate alternate and mean components of complex NP load histories. To accomplish that, the history must first be represented in a two-dimensional (2D) Euclidean sub-space of the transformed 5D deviatoric stress-space $E_{5\sigma}$ (for stress histories) or strain-space $E_{5\varepsilon}$ (for strain histories). These 5D deviatoric spaces represent the stress and strain states using the vectors $\bar{S}'$ and $\bar{e}'$, defined as

$$\bar{S}' \equiv [\,S_1 \quad S_2 \quad S_3 \quad S_4 \quad S_5\,]^T \tag{9}$$

$$\bar{e}' \equiv [\,e_1 \quad e_2 \quad e_3 \quad e_4 \quad e_5\,]^T \tag{10}$$

where

$$S_1 \equiv \sigma_x - \frac{\sigma_y + \sigma_z}{2},\quad S_2 \equiv \frac{\sigma_y - \sigma_z}{2}\sqrt{3},\quad S_3 \equiv \tau_{xy}\sqrt{3},\quad S_4 \equiv \tau_{xz}\sqrt{3},\quad S_5 \equiv \tau_{yz}\sqrt{3} \tag{11}$$

$$e_1 \equiv \varepsilon_x - \frac{\varepsilon_y + \varepsilon_z}{2},\quad e_2 \equiv \frac{\varepsilon_y - \varepsilon_z}{2}\sqrt{3},\quad e_3 \equiv \frac{\gamma_{xy}}{2}\sqrt{3},\quad e_4 \equiv \frac{\gamma_{xz}}{2}\sqrt{3},\quad e_5 \equiv \frac{\gamma_{yz}}{2}\sqrt{3} \tag{12}$$

Note that the 5D stress-space used in the MOI method is a scaled version of the Euclidean space proposed by Papadopoulos et al. in [10].

The MOI method assumes that the 2D load path, represented by a series of points (X, Y) that describe the stress or strain variations along it, is analogous to a homogeneous wire with unit mass. Note that X and Y can have stress or strain units, but they are completely unrelated to the directions x and y usually associated with the material surface. The mean component of the path is assumed, in the MOI method, to be located at the center of gravity of this hypothetical homogeneous wire shaped as the load history path. Such center of gravity is located at the perimeter centroid (X_c, Y_c) of the path, calculated from contour integrals along it

$$X_c = \frac{1}{p_{XY}} \cdot \oint X \cdot dp_{XY},\quad Y_c = \frac{1}{p_{XY}} \cdot \oint Y \cdot dp_{XY},\quad p_{XY} = \oint dp_{XY} \tag{13}$$

where dp_{XY} is the length of an infinitesimal arc of the path and p_{XY} is the path perimeter, see Fig. 3.

Note that this perimeter centroid (PC) is in general different from the area centroid (AC), which is the center of gravity of a uniform density sheet bounded by the shape of the closed path D. The reason to choose the perimeter centroid instead of the area centroid to locate the mean component can be readily seen in the example in Fig. 4. In this example, the right portion of the history

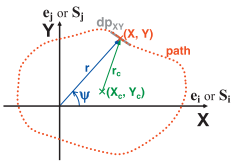

Fig. 3. History path, assumed as a homogeneous wire with unit mass.

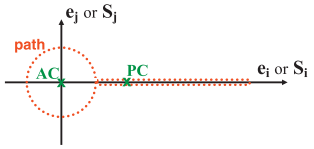

Fig. 4. The area centroid (AC) does not reflect well the mean component of the path D, while the perimeter centroid (PC) is a good measure of such mean.

has almost zero area, therefore it allows the area centroid to be located approximately at the origin of the diagram, which is not physically reasonable for such an asymmetrical path. The perimeter centroid, on the other hand, gives a much more reasonable estimate of the mean component of such stress or strain paths.

As described in [4], the MOI method calculates the equivalent stress or strain ranges of a loading path from the mass Moments Of Inertia (MOI) of its analogous homogeneous wire, calculated with respect to its perimeter centroid. These MOI at the centroid are obtained from the parallel axis theorem applied to the MOI calculated at the origin O of the diagram, given by the contour integrals along the path

$$I^O_{XX} = \frac{1}{p_{XY}} \cdot \oint Y^2 \cdot dp_{XY}, \quad I^O_{YY} = \frac{1}{p_{XY}} \cdot \oint X^2 \cdot dp_{XY},$$
$$I^O_{XY} = I^O_{YX} = -\frac{1}{p_{XY}} \cdot \oint X \cdot Y \cdot dp_{XY} \tag{14}$$

3.2. 5D Deviatoric plastic strain space

In this work, it is proposed that the above equations from the MOI method can be applied to calculate as well the non-proportionality factor F_{np} of a generic multiaxial load path. The presented 5D deviatoric spaces are appropriate to define an integral equation to estimate F_{np} because, contrary to Bishop's method [9], they are independent of the hydrostatic components. However, instead of using the 5D deviatoric stress or strain spaces $E_{5\sigma}$ or $E_{5\varepsilon}$, the deviatoric *plastic* strain space E_{5p} is used to represent the load path, defined as

$$\bar{e}'_p \equiv [\, e_{1p} \quad e_{2p} \quad e_{3p} \quad e_{4p} \quad e_{5p} \,]^T \tag{15}$$

where the subscript p indicates plastic component and

$$e_{1p} \equiv \varepsilon_{x_p} - \frac{\varepsilon_{y_p} + \varepsilon_{z_p}}{2}, \quad e_{2p} \equiv \frac{\varepsilon_{y_p} - \varepsilon_{z_p}}{2}\sqrt{3},$$
$$e_{3p} \equiv \frac{\gamma_{xy_p}}{2}\sqrt{3}, \quad e_{4p} \equiv \frac{\gamma_{xz_p}}{2}\sqrt{3}, \quad e_{5p} \equiv \frac{\gamma_{yz_p}}{2}\sqrt{3} \tag{16}$$

Note that this 5D representation of plastic strains is the same as the one proposed by Tanaka [6] multiplied by a 1.5 scaling factor, since the identity $\varepsilon_{xp} + \varepsilon_{yp} + \varepsilon_{zp} = 0$ implies that $\varepsilon_{yp} - \varepsilon_{zp} = \varepsilon_{xp} + 2\varepsilon_{yp}$.

There are five motivations to use the proposed 5D projection $\bar{e}'_p$ of the plastic strain space to calculate F_{np}: (i) it is a non-redundant representation of the plastic strains, since the linear dependence $\varepsilon_{xp} + \varepsilon_{yp} + \varepsilon_{zp} = 0$ has been removed when projecting the 6D strains onto this 5D sub-space; (ii) similarly to the projections $\bar{S}'$ and $\bar{e}'$, $\bar{e}'_p$ is independent of hydrostatic components, since it is a 5D projection of the deviatoric space as well; (iii) its scaled down version $\bar{e}'_p/1.5$ has been shown by Tanaka [6] to be appropriate to evaluate the non-proportional hardening evolution in incremental plasticity calculations; (iv) the Euclidean norm $|\bar{e}'_p|$ is equal to the von Mises equivalent plastic strain, without the need for any scaling factors; and (v) the direction of such 5D strain vectors is related with the principal direction of the loading. This last statement can be observed, for instance, in the calculation of the principal direction angle θ_p with respect to the y axis in the y–z plane

$$\tan 2\theta_p = \frac{\gamma_{yz}}{\varepsilon_y - \varepsilon_z} = \frac{e_5}{e_2} \cong \frac{e_{5p}}{e_{2p}} \tag{17}$$

where the approximation $e_5/e_2 \cong e_{5p}/e_{2p}$ is valid for large plastic strains, which result in $\bar{e}' \cong \bar{e}'_p$. Therefore, the angle of the strain vector $\bar{e}'$ in the $e_2 \times e_5$ diagram is equal to twice the principal direction θ_p in the y–z plane, making the 5D deviatoric strain vector $\bar{e}'$ (and consequently $\bar{e}'_p$, during plastic straining that causes NP hardening) a good descriptor of the changes in the principal direction. The same arguments can be applied to the principal directions in the x–y and x–z planes, after appropriate coordinate rotations of the vectors $\bar{e}'$ and $\bar{e}'_p$.

Thus, to calculate the directions suffering larger plastic strain magnitudes, the plastic strain path in its E_{5p} space can be imagined as a homogeneous wire with unit mass, as it was assumed before for the $E_{5\sigma}$ and $E_{5\varepsilon}$ stress and strain paths in the original MOI method to calculate the equivalent ranges and mean components. This is physically sound, since the moments of inertia of such unit mass wire with respect to the origin are related to how much the path stretches in each considered direction, and therefore can be correlated with how much accumulated plastic straining there is in such direction. The proposed MOI estimates for F_{np} are detailed next.

3.3. Calculation of F_{np} for 2D load histories

Before generalizing the procedure to a generic 6D multiaxial loading, let's formulate the MOI method to calculate the non-proportionality factor F_{np} of a simple elastoplastic tension–torsion path, which has with non-zero plastic strain components ε_{xp}, γ_{xyp} and $\varepsilon_{yp} = \varepsilon_{zp} = -0.5 \cdot \varepsilon_{xp}$, resulting in

$$e_{1p} \equiv \varepsilon_{x_p} - \frac{\varepsilon_{y_p} + \varepsilon_{z_p}}{2} = \frac{3}{2}\varepsilon_{x_p}, \quad e_{2p} \equiv \frac{\varepsilon_{y_p} - \varepsilon_{z_p}}{2}\sqrt{3} = 0,$$
$$e_{3p} = \frac{\gamma_{xy_p}}{2}\sqrt{3}, \quad e_{4p} = 0, \quad e_{5p} = 0 \tag{18}$$

Since only e_{1p} and e_{3p} are different than zero, the plastic strain path of such tension–torsion history can be represented in the 2D diagram $e_{1p} \times e_{3p} = 1.5 \cdot (\varepsilon_{xp} \times \gamma_{xyp}/\sqrt{3})$, see Fig. 5.

The F_{np} estimate for 2D paths is simply the ratio between the two radii of gyration of the plastic strain path about its principal axes, which is a measure of the aspect ratio of the path and, therefore, of its non-proportionality. The radius of gyration about a given axis can be calculated as the root mean square of the distance between the axis and each point of the path. Since the plastic strain path is assumed to be a wire with unit mass, it follows that the radius of gyration is the square root of the moment of inertia about the desired axis. Therefore, F_{np} is here estimated as the square root of the ratio between the principal axial moments of inertia of the path.

The moments of inertia about the axes $X \equiv e_{1p}$ and $Y \equiv e_{3p}$ are calculated from Eq. (14), giving

$$I^O_{11} = \frac{1}{p} \cdot \oint e^2_{3p} \cdot dp, \quad I^O_{33} = \frac{1}{p} \cdot \oint e^2_{1p} \cdot dp,$$
$$I^O_{13} = I^O_{31} = -\frac{1}{p} \cdot \oint e_{1p} \cdot e_{3p} \cdot dp \tag{19}$$

where dp is the equivalent plastic strain increment and p is the accumulated plastic strain, defined as

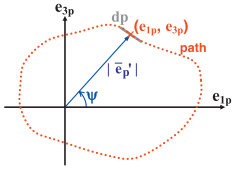

Fig. 5. Plastic strain path in the $e_{1p} \times e_{3p} = 1.5 \cdot (\varepsilon_{xp} \times \gamma_{xyp}/\sqrt{3})$ diagram for a tension–torsion history.

$$dp \equiv \frac{2}{3}\cdot|d\bar{e}'_p| \text{ and } p \equiv \oint dp = \frac{2}{3}\cdot\oint|d\bar{e}'_p| = \frac{2}{3}\cdot(\textit{perimeter}) \tag{20}$$

Note from Eq. (20) that the actual perimeter of the plastic strain path in the $e_{1p}\times e_{3p}$ diagram is equal to $1.5\cdot p$, consequently the length $|d\bar{e}'_p|$ of an infinitesimal arc of the path is $1.5\cdot dp$. The value of the MOI is not changed by the introduction of this scaling factor of 1.5, since it is cancelled in the dp/p ratio; it has been introduced simply to adopt in the formulation the well-known incremental plasticity parameters dp and p instead of $|d\bar{e}'_p|$ and the path perimeter. Defining the 2×2 Axial MOI tensor of the plastic strain path with respect to the origin O as

$$\underline{I}^O = \begin{bmatrix} I^O_{11} & I^O_{13} \\ I^O_{31} & I^O_{33} \end{bmatrix} = \frac{1}{p}\cdot\oint\begin{bmatrix} e^2_{3p} & -e_{1p}\cdot e_{3p} \\ -e_{1p}\cdot e_{3p} & e^2_{1p} \end{bmatrix}\cdot dp \tag{21}$$

then its eigenvalues λ^*_1 and λ^*_2 ($\lambda^*_1 \le \lambda^*_2$) are the moments of inertia about its principal axes, whose directions are parallel to the corresponding eigenvectors, calculated by

$$\lambda^*_{1,2} = \frac{I^O_{11}+I^O_{33}}{2} \pm \sqrt{\left(\frac{I^O_{11}-I^O_{33}}{2}\right)^2 + \left(I^O_{13}\right)^2} \Rightarrow F_{np} = \sqrt{\lambda^*_1/\lambda^*_2} \tag{22}$$

Let's verify the above estimate for a few basic elastoplastic histories, studying the resulting plastic strain paths. A proportional history always results in $F_{np}=0$, as expected, since the resulting plastic strain path is a straight segment passing through the origin O, which has a principal moment of inertia $\lambda^*_1 = 0$ about its own straining direction. A 90° out-of-phase tension–torsion history, on the other hand, always results in $F_{np}=1$, since by symmetry the plastic strain path along the $e_{1p}\times e_{3p}$ plane describes a circular ring, giving $\lambda^*_1 = \lambda^*_2$ Finally, a plastic strain path describing an ellipsis with semi-axes a and b ($a \ge b$) gives

$$F_{np} = \frac{b}{a}\cdot\sqrt{\frac{\int_0^{\pi/2}\sin^2\theta\cdot\sqrt{\sin^2\theta+\left(\frac{b}{a}\right)^2\cos^2\theta}\cdot d\theta}{\int_0^{\pi/2}\sin^2\theta\cdot\sqrt{\cos^2\theta+\left(\frac{b}{a}\right)^2\sin^2\theta}\cdot d\theta}} \cong \frac{b}{a}\,(6.4\%\text{ RMS error}) \tag{23}$$

which agrees within 6.4% with the commonly adopted approximation $F_{np}\cong b/a$.

3.4. Calculation of F_{np} for general load histories

The MOI method to estimate F_{np} is now generalized for a 6D multiaxial history containing all 3 normal and 3 shear components. Once the plastic strain path is obtained, e.g. from incremental plasticity calculations, it must be represented in the five-dimensional E_{5p} space. Note, however, that the Axial MOI (AMOI) used in Section 3.3, which is the moment of inertia of the path about a given axis, is a measure of how much the path stretches in every *other* direction perpendicular to such axis. In order to calculate how much the path stretches along each individual direction, the Rectangular MOI (RMOI) tensor $\underline{I}^O_r$ of the plastic strain path with respect to the origin O is used instead, which gives the moments of inertia about the planes (or hyperplanes) perpendicular to each considered direction:

$$\underline{I}^O_r = \frac{1}{p}\cdot\oint\bar{e}'_p\cdot\bar{e}'^T_p\cdot dp = \frac{1}{p}\cdot\oint\begin{bmatrix} e^2_{1p} & e_{1p}\cdot e_{2p} & e_{1p}\cdot e_{3p} & e_{1p}\cdot e_{4p} & e_{1p}\cdot e_{5p} \\ e_{2p}\cdot e_{1p} & e^2_{2p} & e_{2p}\cdot e_{3p} & e_{2p}\cdot e_{4p} & e_{2p}\cdot e_{5p} \\ e_{3p}\cdot e_{1p} & e_{3p}\cdot e_{2p} & e^2_{3p} & e_{3p}\cdot e_{4p} & e_{3p}\cdot e_{5p} \\ e_{4p}\cdot e_{1p} & e_{4p}\cdot e_{2p} & e_{4p}\cdot e_{3p} & e^2_{4p} & e_{4p}\cdot e_{5p} \\ e_{5p}\cdot e_{1p} & e_{5p}\cdot e_{2p} & e_{5p}\cdot e_{3p} & e_{5p}\cdot e_{4p} & e^2_{5p} \end{bmatrix}\cdot dp \tag{24}$$

The eigenvalues $\lambda_1, \lambda_2, \ldots, \lambda_5$ ($\lambda_1 \ge \lambda_2 \ge \ldots \ge \lambda_5$) of $\underline{I}^O_r$ are a measure of the accumulated plastic strain along each principal direction defined by the associated eigenvectors. The F_{np} estimate is here defined as the as the square root of the ratio between the two largest eigenvalues of $\underline{I}^O_r$, i.e.

$$F_{np} = \sqrt{\lambda_2/\lambda_1} \tag{25}$$

The RMOI and AMOI can be correlated with the help of the Polar Moment Of Inertia (PMOI) I^O_p of the plastic strain path about the origin O, which is a scalar that can be obtained from the trace $tr(\underline{I}^O_r)$ of the RMOI tensor

$$I^O_p = tr(\underline{I}^O_r) = \frac{1}{p}\cdot\oint\left(e^2_{1p}+e^2_{2p}+e^2_{3p}+e^2_{4p}+e^2_{5p}\right)\cdot dp = \frac{1}{p}\cdot\oint\bar{e}^T_p\cdot\bar{e}_p\cdot dp \tag{26}$$

From Eqs. (24) and (25) it can be shown that the AMOI tensor $\underline{I}^O$ can be obtained from the PMOI I^O_p and RMOI $\underline{I}^O_r$ through

$$\underline{I}^O = I^O_p\cdot\underline{I}_{5\times5} - \underline{I}^O_r = \frac{1}{p}\cdot\oint\left(\bar{e}^T_p\cdot\bar{e}_p\cdot I_{5\times5} - \bar{e}_p\cdot\bar{e}^T_p\right)\cdot dp \tag{27}$$

where $\underline{I}_{5\times5}$ is the 5×5 identity matrix. Since the trace of $\underline{I}^O_r$ is always equal to the sum of its eigenvalues, it follows that $I^O_p = \lambda_1+\lambda_2+\lambda_3+\lambda_4+\lambda_5$, and therefore the principal moments of inertia $\lambda^*_1, \lambda^*_2, \ldots, \lambda^*_5$ of the path (the eigenvalues of $\underline{I}^O$, with $\lambda^*_1 \le \lambda^*_2 \le \ldots \le \lambda^*_5$) are a function of the eigenvalues of $\underline{I}^O_r$, namely

$$\lambda^*_i = I^O_p - \lambda_i = \sum_{j\ne i}\lambda_j, \quad \text{for} \quad i = 1,2,\ldots,5 \tag{28}$$

Note that $\underline{I}^O$ and $\underline{I}^O_r$ also share the same eigenvectors. It follows that F_{np} can also be estimated from the PMOI and the two *lowest* principal moments of inertia λ^*_1 and λ^*_2 of the path, since

$$F_{np} = \sqrt{\frac{\lambda_2}{\lambda_1}} = \sqrt{\frac{I^O_p-\lambda^*_2}{I^O_p-\lambda^*_1}} \tag{29}$$

For a 2D (instead of 5D) plastic strain path, where $I^O_p = \lambda_1+\lambda_2$, the principal moments of inertia are $\lambda^*_1 = I^O_p - \lambda_1 = \lambda_2$ and $\lambda^*_2 = I^O_p - \lambda_2 = \lambda_1$, giving $F_{np} = \sqrt{\lambda_2/\lambda_1} = \sqrt{\lambda^*_1/\lambda^*_2}$, proving the equivalence between Eqs. (25) and (22), even though the former is based on the RMOI (also known as the Planar MOI) and the latter on the AMOI.

Even though both the MOI and Bishop's methods estimate F_{np} using similar formulas, shown in Eqs. (25) and (8), their results are quite different, since the former uses the principal RMOI of *deviatoric plastic strain* paths with respect to the *origin O*, while the latter uses the principal RMOI of the *stress* paths with respect to their *mean*.

3.5. Numerical calculation of F_{np}

To implement the MOI method in an incremental plasticity computer code, it is necessary to numerically calculate the integral in Eq. (24) to obtain the RMOI tensor $\underline{I}^O_r$ and then F_{np}. If $\bar{e}'_p$ is the plastic strain vector (in the E_{5p} space) at each calculation step and $\Delta\bar{e}'_p$ is the associated finite plastic strain increment (calculated e.g. from a plastic flow rule), then the RMOI integral can be estimated by a summation based on Simpson's rule [15]

$$\underline{I}^O_r \cong \frac{1}{6p}\cdot\sum\left[\bar{e}'_p\cdot\bar{e}'^T_p + (\bar{e}'_p+\Delta\bar{e}'_p)\cdot(\bar{e}'_p+\Delta\bar{e}'_p)^T + 4\cdot(\bar{e}'_p+\Delta\bar{e}'_p/2)\cdot(\bar{e}'_p+\Delta\bar{e}'_p/2)^T\right]\cdot\Delta p \tag{30}$$

where

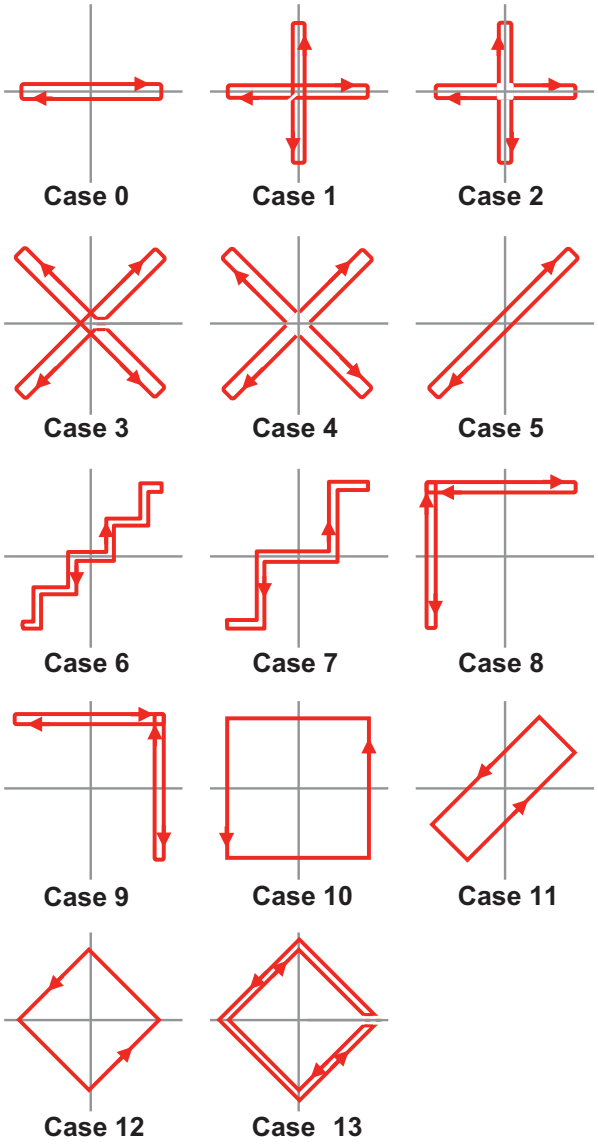

Fig. 6. Strain paths $\varepsilon \times \gamma_{xy}\sqrt{3}$ used in the experimental validation of the F_{np} predictions.

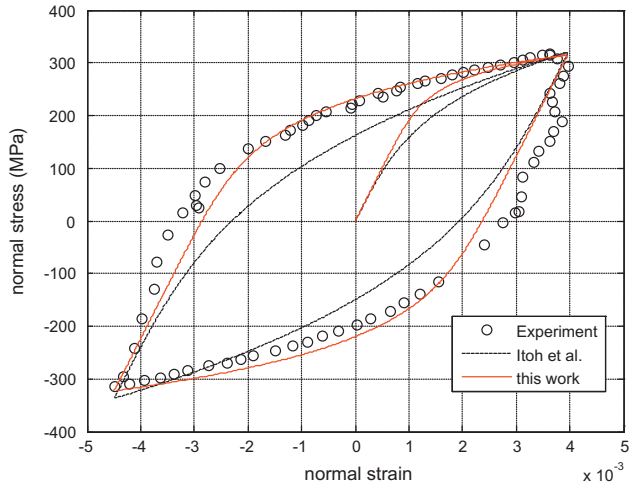

Fig. 7. Ramberg–Osgood equation fitted to the uniaxial hysteresis loops from Case 0, for strain ranges near 0.8%.

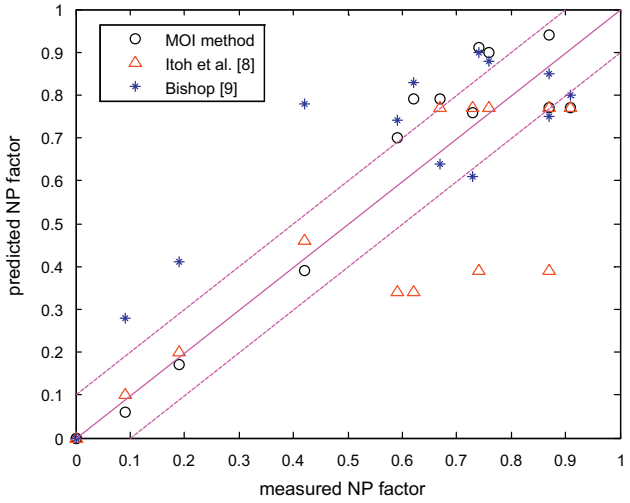

Fig. 8. Measured and predicted F_{np} from the MOI, Itoh's and Bishop's methods, for a 304 stainless steel at strain range levels near 0.8%.

Table 1
Predicted F_{np} from the MOI, Itoh's and Bishop's methods, compared with measured values for a 304 stainless steel at normal strain range levels $\Delta\varepsilon \equiv 0.8\%$.

	Measured	MOI	Itoh et al.	Bishop
Case 0	0.00	0.00	0.00	0.00
Case 1	0.59	0.70	0.34	0.74
Case 2	0.62	0.79	0.34	0.83
Case 3	0.87	0.77	0.39	0.75
Case 4	0.74	0.91	0.39	0.90
Case 5	0.00	0.00	0.00	0.00
Case 6	0.09	0.06	0.10	0.28
Case 7	0.19	0.17	0.20	0.41
Case 8	0.73	0.76	0.77	0.61
Case 9	0.67	0.79	0.77	0.64
Case 10	0.87	0.94	0.77	0.85
Case 11	0.42	0.39	0.46	0.78
Case 12	0.76	0.90	0.77	0.88
Case 13	0.91	0.77	0.77	0.80

$$\Delta p \equiv \frac{2}{3}\cdot|\Delta\bar{e}'_p| \text{ and } p = \sum \Delta p \tag{31}$$

Note that the value of I_r^0 can be computed in real time at each calculation step to obtain, from Eq. (25), the evolution of the target value of F_{np} with the load path. The transient evolution of F_{np} can also be calibrated using the NP hardening rate b_{np}, retarding the transition between $F_{np} = 0$ and the current target value $F_{np} = \sqrt{\lambda_2/\lambda_1}$ through the differential equation

$$dF_{np} = b_{np}\cdot\left(\sqrt{\lambda_2/\lambda_1} - F_{np}\right)\cdot dp \tag{32}$$

Assuming a linear relation between F_{np} and Ramberg–Osgood's hardening coefficient, the constant b_{np} used in the evolution of F_{np} can be calibrated using the same value as the hardening rate from Tanaka's cyclic plasticity model [16].

4. Comparisons among F_{np} predictions

The MOI, Itoh's and Bishop's methods' predictions of the non-proportionality factor F_{np} are now compared to experimental measurements from Itoh et al. [8,11] in a 304 stainless steel with Young's modulus $E = 200$ GPa, shear modulus $G = 82$ MPa and additional hardening coefficient $\alpha_{np} = 0.9$. Fourteen periodic histories are studied, represented by the strain paths $\varepsilon \times \gamma_{xy}/\sqrt{3}$ shown in Fig. 6 for Cases 0 through 13. Note that most loadings from Fig. 6

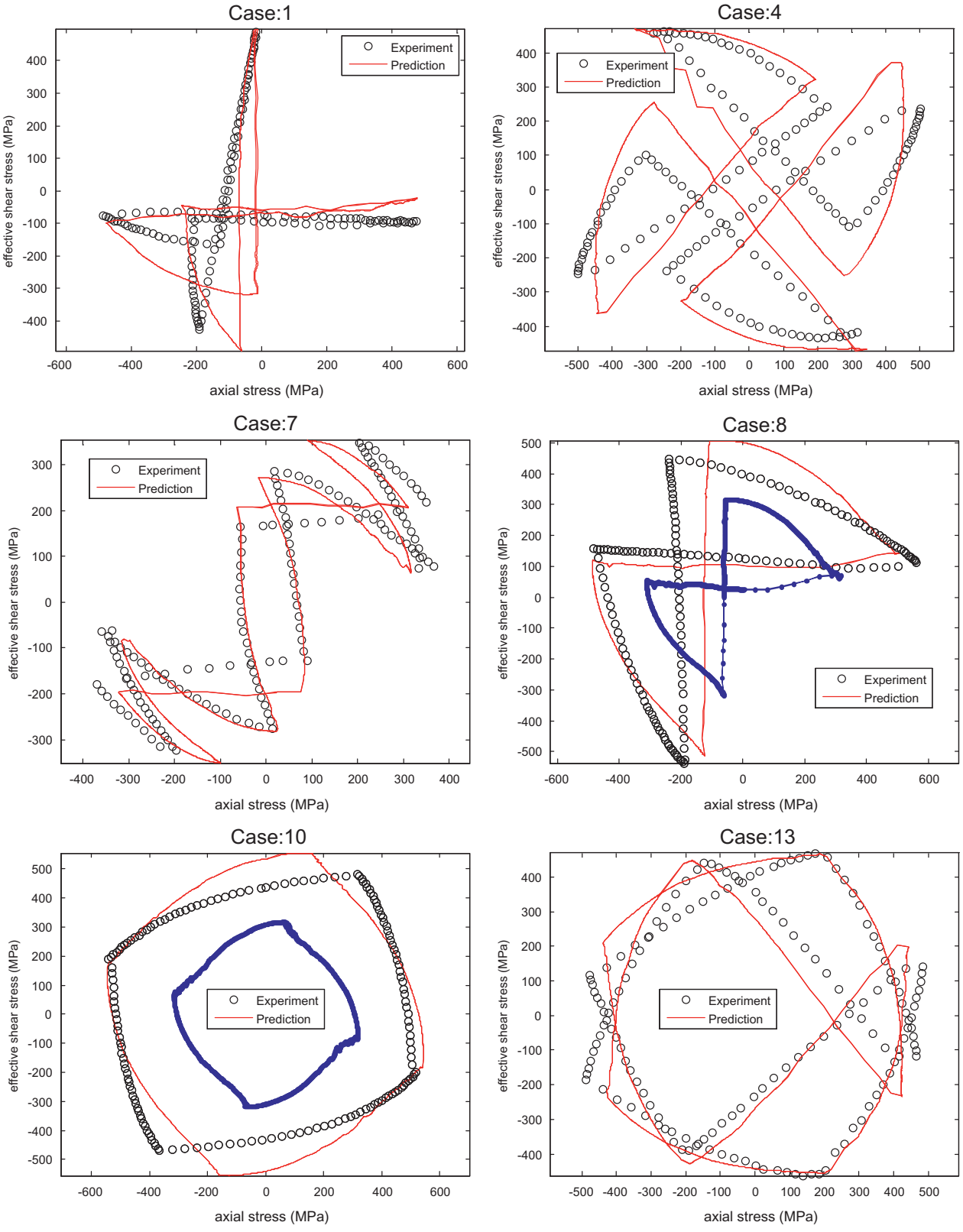

Fig. 9. Experimental values and *predictions* of the stress paths $\sigma \times \tau\sqrt{3}$ using the MOI method applied to Jiang's incremental plasticity model for Cases 1, 4, 7, 8, 10 and 13. The thicker solid lines in Cases 8 and 10 represent wrong predictions that would be obtained if the effect of F_{np} on the additional hardening had been neglected.

consider one cycle per block, except for Cases 1 through 4 and Case 13, which consider two cycles per block. The number of cycles in each block can be deterministically obtained using the Modified Wang Brown rainflow algorithm, described in [3]. The normal strain range $\Delta\varepsilon$ of all studied experimental data is fixed near 0.8%, to avoid issues with the strain amplitude dependence of α_{np}.

Fig. 7 shows the curve fitting of the Ramberg–Osgood equation to the uniaxial hysteresis loops from Case 0 with $\Delta\varepsilon \equiv 0.8\%$,

resulting in a uniaxial cyclic hardening coefficient $k' = 670$ MPa and exponent $n' = 0.125$. Note that the curve fitting used by Itoh et al. [8,11], also shown in the figure, does not reproduce well the shape of the hysteresis loops measured for $\Delta\varepsilon \equiv 0.8\%$, most likely because it had been calibrated from uniaxial data with $\Delta\varepsilon \equiv 1.5\%$ [11].

To evaluate the F_{np} predictions, an incremental plasticity computer code is implemented using Jiang's non-linear kinematic model [12]. To improve the calculation accuracy, the backstress is divided into 50 additive components, following Chaboche's idea [13], with stress increments at each integration step limited to only 2 MPa. Jiang's material parameters are calibrated from the uniaxial data using the procedure described in [14], neglecting transient ratcheting effects. The computer code accuracy is verified using the same model in both stress and strain control, as recommended in [1]. That is, the stress history is calculated in the code from a given strain history, and then the computed stresses are used as input to the same code to predict the original strain history, with residual errors smaller than 0.1% for the adopted numerical integration parameters.

For each strain-controlled loading case, the incremental plasticity code is iteratively executed for several candidate values of F_{np}, until the root mean square (RMS) error between the calculated and the measured strain paths in the $\sigma \times \tau\sqrt{3}$ diagram is minimized. The value of F_{np} that minimizes the RMS error for each of the 14 paths is assumed to be the experimental non-proportionality factor, which is compared in Fig. 8 with the MOI, Itoh's and Bishop's predictions. As shown in Table 1, the MOI method predicts in average better values for F_{np} than Itoh's and Bishop's method. Itoh's method highly underestimates F_{np} for star or cross-shaped histories such as the ones from Cases 1 through 4. Bishop's method, on the other hand, overestimates roughly by a factor of 2 or more the non-proportionality factors of loading histories with $0 < F_{np} < 0.5$ (Cases 6, 7 and 11), for the same reason discussed in the example from Fig. 1(d).

Fig. 9 shows experimental stress paths $\sigma \times \tau\sqrt{3}$ and the incremental plasticity predictions using Jiang's model and the MOI method to estimate F_{np}. Note that the solid curves are *predictions* based solely on uniaxial values, on α_{np} and on MOI's F_{np} estimates, they are not curve fittings. It can be seen that both the shape and the amplitudes of the stress paths are reasonably predicted using the F_{np} estimates from the MOI method. The additional hardening effect is very significant in all measured non-proportional paths, as it can be seen in Cases 8 and 10, which also show the resulting non-conservative predictions if the effect of F_{np} had been neglected, which would severely underestimate both normal and shear stresses.

5. Conclusions

The MOI method is an alternative to convex enclosure methods to obtain equivalent amplitude or range and mean components of generic NP multiaxial histories, in addition to efficiently predicting the non-proportionality factor F_{np}, without the need for adjustable parameters. Convex enclosure methods do not represent well F_{np} or the mean component of a path, in special if it has a very odd shape, as shown in Fig. 1. The MOI method, on the other hand, accounts for the contribution of every single segment of the path, dealing with arbitrarily shaped histories without losing information about their shape. Therefore, the MOI method can be successfully used even in highly non-convex stress or strain NP history paths such as cross or star-shaped paths. It is relatively simple, intuitive, and easy to implement and to compute, therefore it should be considered as an alternative engineering tool to deal with NP histories. Coupled with an efficient multiaxial rainflow algorithm, it is able to deal with very long variable amplitude histories.

The MOI method predicts the out-of-phase extent of a loading history based on the eigenvalues λ_i ($i = 1, \ldots, 5$) of the Rectangular Moment Of Inertia (RMOI) tensor of the plastic strain path. This measure of F_{np} is independent of the particular choice of coordinate system, being invariant under coordinate transformations as required. The eigenvectors of the RMOI represent the principal axes of the tensor path with respect to the origin, which may be used as a 'reference frame' for defining the desired non-proportional and out-of-phase measure of the plastic strain path. Even though the proposed F_{np} estimate is only based on the two largest eigenvalues λ_1 and λ_2, improved equations might make use of all 5 eigenvalues to account for the interactions among all principal straining directions.

Experimental results demonstrated the effectiveness of the MOI method for all fourteen studied cases when compared to Itoh's and Bishop's F_{np} estimates. Itoh's method works well for simple 2D histories (e.g. tension–torsion), however it highly underestimates the F_{np} of cross or star-shaped load paths, while overestimating the F_{np} of paths similar to the one from Fig. 1(d). Also, its definition in the time domain is not appropriate, since transient elastoplasticity effects depend on the accumulated plastic strain, independently of time. Unless significant viscous effects are present, Itoh's integral must assume a constant plastic strain rate to eliminate its time dependence. Also, as discussed in Section 2, Itoh's method should not be applied to more general 3D to 6D histories, since it is based on a scalar measure, the angle $\xi(t)$, which is not enough to represent all possible variations of the principal direction (which are well described e.g. by the 5 pairs of eigenvalues and eigenvectors of the RMOI).

Bishop's approach also results in poor predictions, in special for histories with $0 < F_{np} < 0.5$. Despite using the promising concept of the RMOI, Bishop's estimate is formulated in a stress space (instead of a plastic strain space), it implicitly assumes a hydrostatic dependence of F_{np}, and it calculates the moments of inertia relative to the mean component of the load path instead of the origin, which would wrongfully predict $F_{np} = 0$ for the path from Fig. 1(c).

Acknowledgments

The authors would like to acknowledge Prof. Darrell F. Socie for providing the experimental data from [8].

References

[1] Socie DF, Marquis GB. Multiaxial Fatigue. SAE 1999.
[2] Langlais TE, Vogel JH, Chase TR. Multiaxial cycle counting for critical plane methods. Int J Fatigue 2003;25:641–7.
[3] Meggiolaro MA, Castro JTP. An improved multiaxial rainflow algorithm for non-proportional stress or strain histories – Part II: The modified Wang-Brown method. Int J Fatigue 2012;42:194–206.
[4] Meggiolaro MA, Castro JTP. An improved multiaxial rainflow algorithm for non-proportional stress or strain histories – Part I: Enclosing surface methods. Int J Fatigue 2012;42:217–26.
[5] Shamsaei N, Fatemi A. Effect of microstructure and hardness on non-proportional cyclic hardening coefficient and predictions. Mater Sci Eng A 2010;527:3015–24.
[6] Tanaka E. A non-proportionality parameter and a cyclic viscoplastic constitutive model taking into account amplitudedependences and memory effects of isotropic hardening. Eur J Mech – A/Solids 1994;13:155–73.
[7] Kanazawa K, Miller K, Brown M. Cyclic deformation of 1% Cr–Mo–V steel under out-of-phase loads. Fatigue Fract Eng Mater Struct 1979;2:217–28.
[8] Itoh T, Sakane M, Ohnami M, Socie DF. Nonproportional low cycle fatigue criterion for type 304 stainless steel. ASME J Eng Mater Technol 1995;117:285–92.
[9] Bishop JE. Characterizing the non-proportional and out-of-phase extend of tensor paths. Fatigue Fract Eng Mater Struct 2000;23:1019–32.
[10] Papadopoulos IV, Davoli P, Gorla C, Filippini M, Bernasconi A. A comparative study of multiaxial high-cycle fatigue criteria for metals. Int J Fatigue 1997;19:219–35.

[11] Kida S, Itoh T, Sakane M, Ohnami M, Socie DF. Dislocation structure and non-proportional hardening of type 304 stainless steel. Fatigue Fract Eng Mater Struct 1997;20:1375–86.
[12] Jiang Y, Sehitoglu H. Modeling of cyclic ratchetting plasticity, Part I: Development of constitutive relations. ASME J Appl Mech 1996;63(3):720–5.
[13] Chaboche JL, Dang Van K, Cordier G, Modelization of the strain memory effect on the cyclic hardening of 316 stainless steel. In: Transactions of the Fifth International Conference on Structural Mechanics in Reactor Technology, Div. L, Berlin, 1979.
[14] Jiang Y, Sehitoglu H. Modeling of cyclic ratchetting plasticity, Part II: Comparison of model simulations with experiments. ASME J Appl Mech 1996;63(3):726–33.
[15] Atkinson KE. An introduction to numerical analysis. 2nd ed. John Wiley & Sons; 1989.
[16] LeMaitre J. Handbook of materials behavior models. Deformations of materials, vol. I. Academic Press; 2001.